MICROSTRUCTURE-BASED COMPUTATIONAL FATIGUE LIFE PREDICTION OF POLYCRYSTALLINE ALLOYS

Xijia Wu[1], Siqi Li[2], Zhong Zhang[1] and Rong Liu[2]

[1] Aerospace Research Centre, National Research Council Canada, Canada.
Xijia.wu@nrc-cnrc.gc.ca/Zhong.zhang@nrc-cnrc.gc.ca
[2] Department of Mechanical and Aerospace Engineering, Carleton University, Canada. SiqiLi4@cmail.carleton.ca/Rong.Liu@carleton.ca

Abstract: Aircraft structural integrity (ASI) is always facing the challenge of fatigue characterization with scattering of material properties. Traditionally, this is assessed through a statistically significant amount of physical testing, which prolongs the cycle of product development and increases the cost significantly. This research explores a microstructure-based fatigue modelling approach to predict the low cycle fatigue (LCF) crack nucleation life of polycrystalline materials, using the nickel-based alloy Haynes 282 as an example. A three-dimensional representative volume element (RVE) consisting of polycrystalline aggregates is constructed for the material using Voronoi tessellation with the grain size distribution from microstructural analysis and grain orientations randomly assigned for isotropy. Hill's yield criteria and linear strain hardening are employed to describe the anisotropic plasticity of each grain, using a finite element method (FEM), such that the overall deformation response matches the cyclic hysteresis behaviour of Haynes 282 alloy at the macroscopic scale. The fatigue crack nucleation life of Haynes 282 alloy is predicted using the Tanaka Mura Wu (TMW) model based on the material surface energy, shear modulus, Burgers vector, and the microstructural plastic strain range. The fatigue crack growth life under LCF conditions is described using the Tomkins equation. It is demonstrated that this approach can computationally predict the fatigue life of Haynes 282 alloy and estimate the scattering of the fatigue life through simulations with different sets of the grain distribution functions. The model predictions are in good agreement with the coupon tests, in a statistical sense.

Keywords: Fatigue life prediction, Microstructure, Representative volume element (RVE), Polycrystalline material, Finite element method (FEM).

INTRODUCTION

The theme of ICAF2023 is Aircraft Structural Integrity (ASI) in a World in Transition. This requires an enhanced version of ASI utilizing more reliable modelling and simulation, as well as artificial intelligence. The traditional structural integrity programs rely heavily on fatigue testing to characterize the effects of many factors including composition and microstructure (grain size, orientation, precipitates and inclusion), manufacturing defects; part geometry (shape and size), surface finish, residual stress etc., which may be experienced by components in service under variable loading [1]. The

critical challenge in ASI is to quantify the effect and scattering of each factor in the structural design and aircraft maintenance. In certification, the FAA AC 25.571-1D requires that a) material fatigue scatter be investigated to define the limit of 99% of survival at 95% confidence; b) the statistical variation and severity of mission spectrum be fully accounted for, and c) a significant number of representative specimen tests be conducted at all levels of the certification pyramid. The traditional way to comply with these requirements is through physical fatigue testing. As most of the aforementioned factors are stochastic, it requires a tremendous amount of testing, which certainly increases the design cost and prolongs the development cycle to market. Recently, certification by analysis (CbA) has been advocated by the aviation industry, as a possible means of compliance, to save both time and cost of aeronautical product development [2]. For CbA of fatigue, the questions are what effects and on what level (coupon, element, component and full scale) can be computationally certifiable with uncertainty quantification (UQ).

The fatigue mechanism, which is well understood, is the cyclic deformation via alternating slip occurs at the microstructural level, and the microstructure has batch-to-batch variability through manufacturing, the UQ for fatigue must be investigated starting at the microstructural level. UQ at higher levels, i.e., coupon, element, component and full scale, involves the effects of local stress triaxiality, stress gradient, and surface finish/residual stress/assembly constraints, etc. on top of the microstructural effect. Therefore, CbA for fatigue is a progressive process through all the levels of the certification pyramid.

The microstructural effects on fatigue have been a topic of many studies in recent years [3-11]. Finite element method (FEM) simulations have been carried out using the meso-level representative volume elements (RVEs) in conjunction with various fatigue models such as Tanaka-Mura model, Fine-Bhat model, and Fatemi-Socie model, for fatigue life prediction. The Tanaka-Mura model uses stress and "specific fracture energy" to specify the criterion of the crack initiation [12]. The Fine and Bhat model also uses an energy criterion with an energy-efficiency factor [13]. The Fatemi-Socie model defines a critical fracture plane [14]. However, all these models need to fit to an experimental S-N curve to determine their parameters. Hence, they are unable to determine the fatigue scatter independently, as the model's confidence level really relies on the coupon failure probability and confidence level of the data for calibration.

Recently, Wu [15] modified the Tanaka-Mura model and re-derived the fatigue crack nucleation life based on the true plastic strain of dislocation pileup. It is hereafter called the Tanaka-Mura-Wu (TMW) model. It has been demonstrated for many pure metals and engineering alloys with fatigue life prediction with material physical properties such as elastic modulus, Poisson's ratio, Burgers vector, surface energy, the applied stress or plastic strain range. The model has been found in good agreement with experimental data [16,17]. Hence, the TMW model promises to provide class-A prediction (forecast before the event occurs), as it does not need calibration to prior fatigue failure data.

In this study, an approach using FEM/RVE/TMW model is outlined to compute fatigue life of Haynes 282 alloy as a demonstration. Haynes 282 is a newly-developed nickel-based superalloy, which is intended to be used in advanced ultra-supercritical (A-USC) steam turbines for power-generation. The RVE microstructure model of the material is constructed using Voronoi tessellation and FEM. Within each grain, the elastic deformation follows the generalized Hooke's law and the plastic deformation is controlled by Hill's potential coupled with linear kinematic hardening. The fatigue damage driver is the equivalent plastic strain magnitude in the microstructure, corresponding to the LCF mechanism. To evaluate the scatting of fatigue life, 20 sets of random grain orientations are assigned to the RVE to represent the random orientation distribution in the microstructure. The predicted fatigue crack nucleation life of Haynes 282 and its scattering are compared with the experimental data.

EXPERIMENT

A Haynes 282 forging is used in this study, which has a norminal composition as given in Table 1. The material received a standard heat treatment (solution treatment at 1121 – 1149℃, followed by aging at 1010℃ for 2 hours, air cooled, and 780℃ for 8 hours, air cooled). It has a face-centered cubic (fcc) γ

solid solution matrix and ordered γ' ($Ni_3(Al, Ti)$) precipitates. The grain size distribution and grain orientation distribution (no texture in this material) are characterized using metallurgical means (optical and scanning electron microscopy), as shown in Figure 1.

Table 1: Nominal composition (wt.%) of Haynes 282 alloy

Ni	Cr	Co	Mo	Ti	Al	Fe	Mn	Si	C	B	Others
Bal.	20	10	8.5	2.1	1.5	1.5*	0.3*	0.15*	0.06	0.005	--

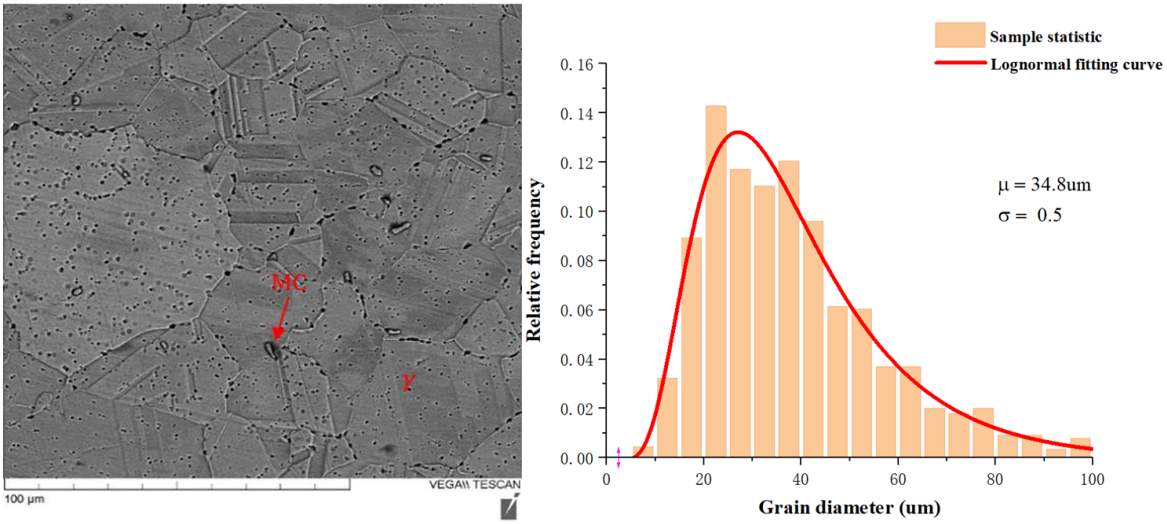

Figure 1: Material microstructure and grain size distribution.

Fully-reversed strain-controlled fatigue tests were conducted at room temperture on an MTS servohydraulic load frame, following ASTM Standard E606. Both incremental step (IS) and constant-amplitude (CA) cyclic tests were conducted using a triangular wave form (R = -1) at a strain rate of 2×10^{-3} s^{-1}. The IS cyclic test was to generate a series of stablilized hysteresis loops with one coupon for material constitutive law, while the CA cyclic tests were to generate fatigue life data for validation.

MICROSTRUCTURE MODELLING

To start, the microstructural information (Figure 1) was inserted into the Dream3D software to generate a three-dimensional (3D) microstructural geometry model. The RVE is built as a volume of 500 × 500 × 500 μm containing 625 grains, which is sufficient for truthful representation of the grain structure of the bulk material, according to the study of Brommesson et al. [18], while computationally efficient. As Dream3D meshes the RVE with brick elements, the grain boundaries appear to be staircases at first. Then, an in- house code was used to re-mesh the RVE with tetrahedron elements so that grain boundaries appear to be "smooth". The final meshed RVE is shown in Figure 2. The γ' precipitates are not explicitly considered in the RVE, because they are extremely small in size and coherent with the γ matrix in Haynes 282. The strengthening effect of γ' precipitates is taken into account in the reference yield stress of Hill's criteria. Fatigue cracks rarely nucleate at the γ/γ' interface, as dislocations would cut through rather than pile-up at the precipitate. The carbides are not considered in the RVE either for this study, since they do not contribute to the fatigue failure of Haynes 282 [19].

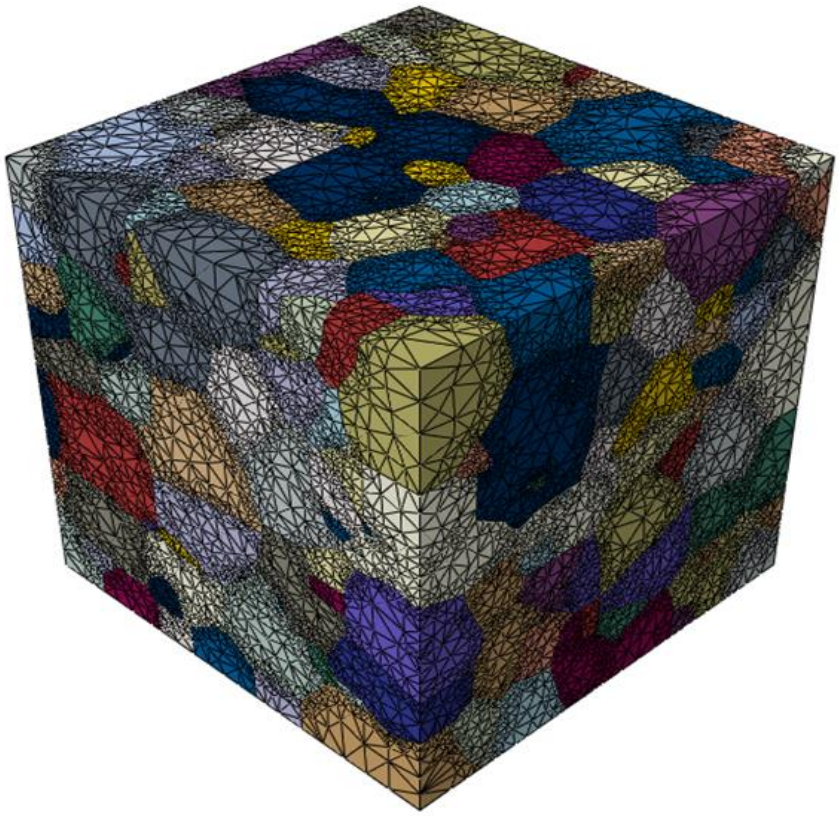

Figure 2: Meshed RVE of Haynes 282.

In order to characterize the effect of grain orientation on the scattering of predicted fatigue life for Haynes 282 alloy, grain orientations with 20 random distribution functions are assigned to individual grains for the RVE model, and FEM simulations have been performed for LCF. In ABAQUS, an arbitrary grain orientation is created by altering the x, y, z components of coordinate axes in the range of [-1, 1] to define the local coordinate system for each grain.

RESULTS AND DISCUSSION

RVE cyclic stress-strain behaviour

In an RVE, each grain behaves in an anisotropic manner. The elastic behaviour of a crystallite follows the generalized Hooke's law: i.e., $\sigma_{ij} = C_{ijkl}\varepsilon_{kl}$. For the plastic deformation, Hill's yield potential is used to describe the overall effect of anisotropic yielding [20]

$$f(\sigma) = \sqrt{F(\sigma_{22} - \sigma_{33})^2 + G(\sigma_{33} - \sigma_{11})^2 + H(\sigma_{11} - \sigma_{22})^2 + 2L{\sigma_{23}}^2 + 2M{\sigma_{31}}^2 + 2N{\sigma_{12}}^2} \quad (1)$$

where *F*, *G*, *H*, *L*, *M* and *N* are material constants that can be determined via tensile tests of the material in different directions. In ABAQUS, the anisotropic yield constants are expressed in terms of the yield stress ratio R_{ij} with a referrence yield stress σ^o. Because of cubic symmetry of the fcc crystal, $F = G = H$, and $L = M = N$, so $R_{11} = R_{22} = R_{33}$ and $R_{23} = R_{13} = R_{12}$. The yield stress ratios are crystalline properties, which are taken from literature [21], while the reference yield stress σ^o is the absolute yield strength of the material, which implicitly includes the solid solution and precipitate hardeing effect.

A linear kinematic hardening rule is used to describe the translation of the center of the current yield surface in the stress space during cyclic loading. This means that the evolution of the back stress tensor ($d\alpha$) follows the Prager's rule [22]:

$$d\alpha = Cd\varepsilon^p \quad (2)$$

where C is the hardening parameter, ε^p is the equivalent plastic strain. According to Eqns. 1 and 2, the material behavior is only controlled by C and σ^o. The size of the initial yield surface σ^o, that is, the reference yield stress, and linear kinematic hardening parameter C are determined through iterative calibration to the macroscopic stress - strain behavior of Haynes 282 alloy.

Here, σ_{ij} and ε_{ij} are the stress/strain components in the local crystallographic system, which are transformed to the global coordinate system, back and forth by tensor transformation, to obtain the global stress – strain $[\sigma']$-$[\varepsilon']$ response.

To simulate the uniaxial loading condition as in coupon testing, the x-direction displacement boundary condition is applied on x = 500 μm side of the RVE, while the displacements in the x direction of all nodes on the opposite boundary plane x = 0 are constrained to zero, so that the entire RVE deforms with a mesoscale uniform strain. The simulated hysteresis loops are shown in Figure 3, which are in very good agreement with the experimental observation. It is interesting to note that although the microstructural yielding is depicted by an elastic-plastic bi-linear function, the macroscopic stress - strain behaviour exhibits a smooth transition from elastic to plastic behaviour, as individual grains experience yielding and stress transfer to neighbour grains. The calibration demonstrates that the RVE can represent the macroscopic hysteresis behavior of Haynes 282. The stress and plastic strain distribution in the RVE is shown in Figure 4.

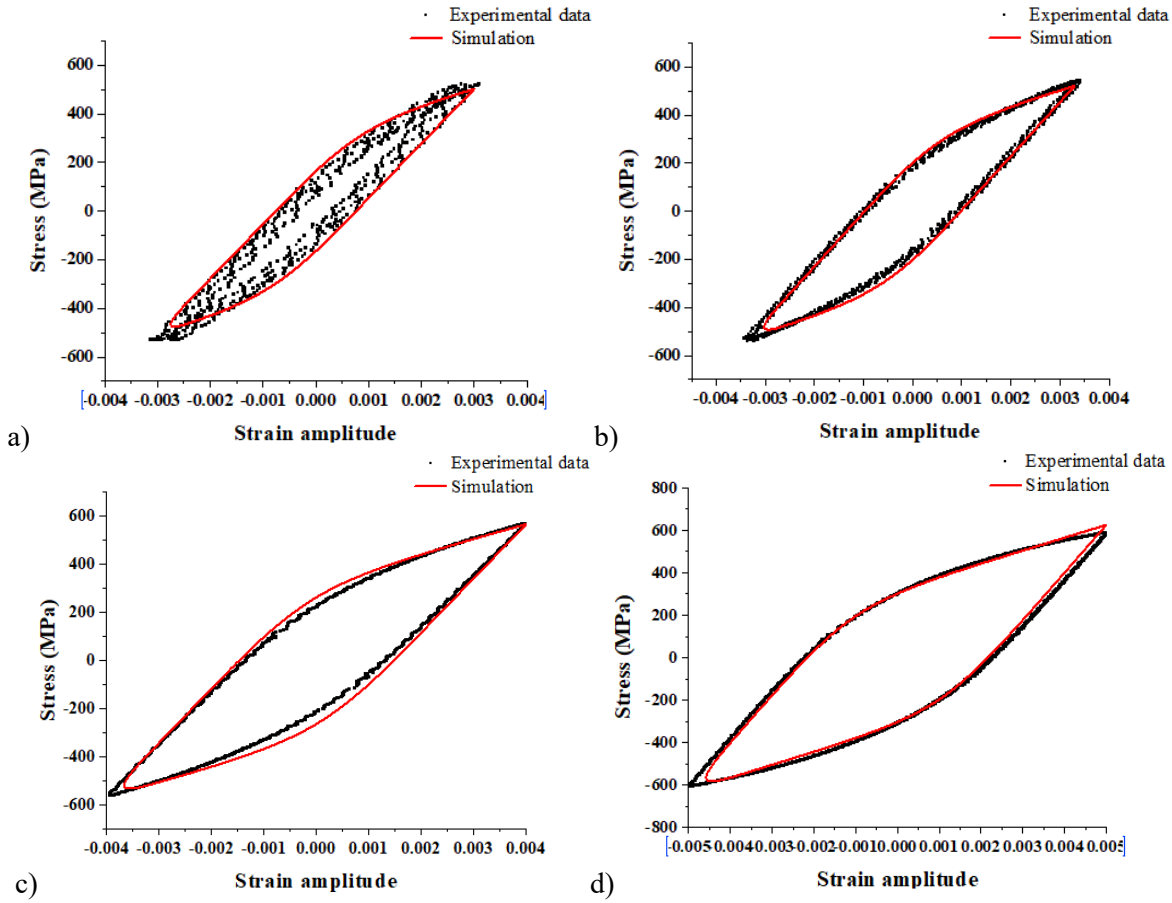

Figure 3: Hysteresis of Haynes 282.

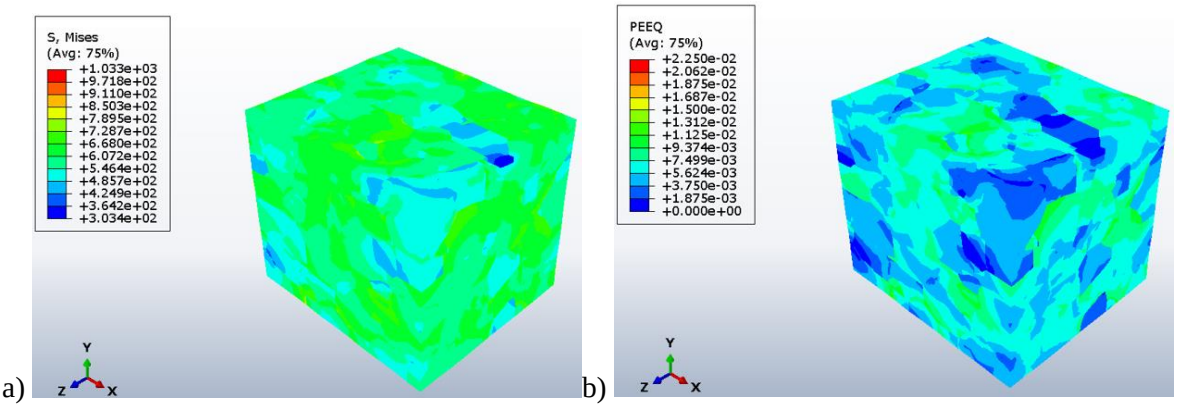

Figure 4: (a) Stress distribution and (b) plastic strain distribution in RVE with $\Delta\varepsilon$ = 0.8%.

Fatigue crack nucleation

At the microstructure level, the TMW model [15] is adopted, which depicts dislocation dipoles pileup, leading to fatigue crack nucleation with a life as given by

$$N_c = \frac{8(1-\nu)R_s w_s}{3\mu b}\Delta\varepsilon_p{}^{-2} \tag{3}$$

where μ is the shear modulus, w_s is the surface energy, ν is Poisson's ratio, b is Burgers vector, R_s is surface roughness factor (R_s = 1 for ideally smooth surface, ~1/3 for machined surface), $\Delta\varepsilon_p$ is the plastic strain range. In ABAQUS, the plastic strain magnitude (PEMAG) is evaluated as $\varepsilon_p = \sqrt{\frac{2}{3}\varepsilon^{pl}:\varepsilon^{pl}}$, which is the product of plastic strain tensor. Eqn. 3 has been validated for many metals and alloys with known elastic modulus, Burgers vector and surface energy values [15-17].

Since crack nucleation preferably occurs at the locations of high localized plastic strain, the element with the maximum plastic strain range in the RVE is assumed to be the first crack nucleation site, the value is inserted into Eqn. 3 to calculate the fatigue crack nucleation life. Note that the elements on the loaded and constrained planes (x = 500 μm and x = 0 μm) are excluded because of the boundary effect.

Fatigue crack growth

For fatigue crack growth analysis, the Tomkins model [23] is adopted, which describes the short fatigue crack growth rate as

$$\frac{da}{dN} = \frac{\pi^2}{8}\left(\frac{\Delta\sigma}{2\sigma_T}\right)^2 \frac{\Delta\varepsilon_p}{(2n+1)}a \tag{4}$$

where σ_T is the ultimate tensile strength of the material and n is the strain hardening exponent.

Eqn. 4 takes into account the effect of plastic strain on fatigue crack growth, as plastic deformation is involved in LCF. Since microscopic crack growth through each individual grains along its path is very tedius to follow, the macroscopic plastic strain is used as evaluated by the Ramberg-Osgood equation for average fatigue crack growth rate.

Total fatigue life

The total fatigue life for a conventional fatigue coupon is thus evaluated as

$$N_f = N_c + N_g \tag{5}$$

where N_c is the crack initiation life calculated by Eqn. 3 and N_g is obtained by integration of Eqn. 4 from the crack nucleation element size to the critial crack size at fracture.

The predicted total fatigue life is shown in Figure 5, in comparison with the experimental data. There is good agreement between the predicted and experimental LCF data, even without prior calibration. At medium to low strain amplitudes, the calculated fatigue life appears to be near the lower-bound of the experimental data. This is partly because the absolute maximum plastic strain value is used in the computation, which could be exacerbated by local element distortion, and partly because no microstructural crack growth retardation is considered. Here, the experimental median line is drawn using the Coffin-Manson equation, and the 95% confidence band is computed according to ASTM E739 [24]. To assess the statistical nature of microstructural effect, the calculated RVE fatigue life is normalized by the theoretical fatigue life given by Eqn. 5 based on the macroscopic plastic strain. The statistical distribution of the microstructural effect is found to be Gaussian, as described by

$$p(x) = \frac{1}{\sigma\sqrt{2\pi}} e^{-\frac{1}{2}\left(\frac{x-\mu}{\sigma}\right)^2} \tag{6}$$

where $x = N/N_{norminal}$ ($N_{norminal}$ is the norminal fatigue life calculated using Eqns. 3 to 5 with plastic strain as evaluated by the Ramberg-Osgood equation).

Eqns. 3 to 6 in combination with the RVE/FEM analysis together offer a computational approach to statistically characterize the effect of microstructure on fatigue life, which can be used to define the fatigue design limit at 99% survival rate with 95% confidence. The demonstration shown in this paper is still premliminary with limited data. Further microstrctrual model refinement is needed as the simulation goes into HCF regime, since the microplastic strain accumulation is very sensitive to element meshing. Nonetheless, the approach is very promissing for fatigue CbA at all levels when combined with structural stress/strain analysis, which can be a huge cost saver for airframe design and certification.

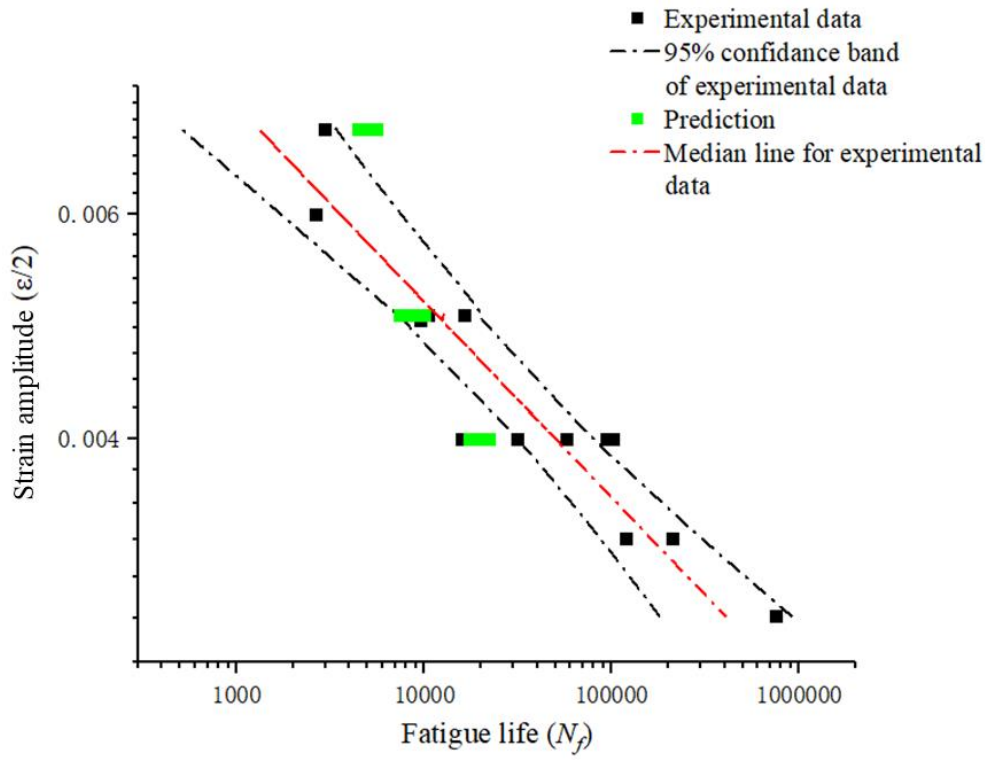

Figure 5: Predicted fatigue life in comparison with the coupon experimental life.

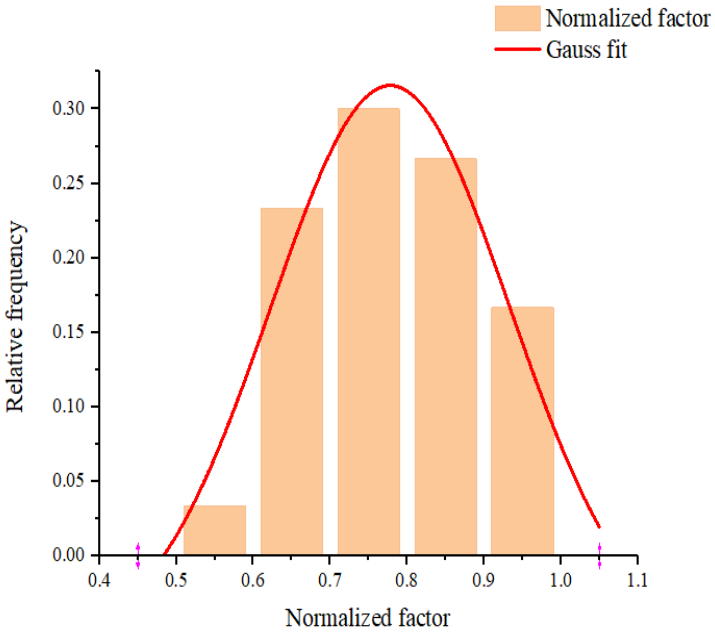

Figure 6: Predicted fatigue life distribution.

CONCLUSIONS

A microstructure-based fatigue modelling approach is proposed to predict the low cycle fatigue (LCF) of polycrystalline materials, using nickel-based alloy Haynes 282 as an example in this paper. The approach consists of

- Building a 3D RVE consisting of polycrystalline aggregates for the material using Voronoi tessellation with the grain size and grain orientation distribution from the real material.
- Using the generalized Hooke's law and Hill's yield criteria/linear strain hardening to describe the anisotropic elastic-plastic behaviour of each grain in the RVE/FEM model, such that the overall deformation response matches the material's macroscopic hysteresis behaviour.
- Calculation of fatigue crack nucleation life using the TMW model with the material surface energy, shear modulus, Burgers vector, and the plastic strain range at the microstructural level.
- Calculation of fatigue crack growth life under LCF conditions using the Tomkins equation.

It is demonstrated that this approach can computationally predict the fatigue life of Haynes 282 alloy and estimate the lower-bound of scattering of fatigue life. The model predictions are in good agreement with the coupon tests.

ACKNOWLEDGEMENT

The authors are grateful for the financial support from the Natural Science & Engineering Research Council of Canada (NSERC) and the in-kind support from the Aeronatical Product Development and Certification program of National Research Council Canada (NRC). In particular, the authors are in debt to the technical officer, Mr. Ryan MacNeil, of NRC for conducting the fatigue tests.

REFERENCES

[1] Schijve, J. (2009), *Fatigue Tests and Scatter, Fatigue of Structures and Materials*, Springer, New York, p. 373.
[2] Olivares, G. Acosta, J.F. and Yadav, V. (2010), *Certification by Analysis I and II*, Computational Mechanics Laboratory, National Institute for Aviation Research Wichita.
[3] McDowell, D.L. (2007), *Mater. Sci. Eng. A*, vol. 468-470, p. 4.
[4] McDowell, D.L. and Dunne, F.P.E. (2010), *Int. J. Fatigue*, vol. 32, n. 9, p. 1521.
[5] Yeratapally, S.R., Glavicic, M.G. Hardy, M. and Sangid, M.D. (2016), *Acta Mater*., vol. 107, p. 152.
[6] Briffod, F., Shiraiwa, T. and Enoki, M. (2016), *Mater. Trans*., vol. 57, n. 10, p. 1741.
[7] Li, L., Shen, L. and Proust, G. (2015), *Mech. Mater*., vol. 81, p. 84.
[8] Ou, C.Y., Voothaluru, R. and Liu, C.R. (2020), *Crystals*, vol. 10, n. 10, p. 1.
[9] Yuan, C.J., Zhang, X.C., Chen, B., Tu, S.T. and Zhang, C.C. (2020), *J. Mater. Sci. Technol*., vol. 38, p. 28.
[10] Cruzado, A., Lucarini, S., Lorca, J. L. and Segurado, J. (2018), *Int. J. Fatigue*, vol. 113, p. 236.
[11] Prithivirajan, V. and Sangid, M.D. (2020), *Mater. Sci. Eng. A*, vol. 783, 139312.
[12] Tanaka, K. and Mura, T. (1981), *J. Appl. Mech*., vol. 48, n. 1, p. 97.
[13] Fine, M.E. and Bhat, S.P. (2007), *Mater. Sci. Eng. A*., vol. 468-470, p. 64.
[14] Fatemi, A. and Socie, D.F. (1988), *Fatigue Fract. Eng. Mater. Struct*., vol. 11, p. 149.
[15] Wu, X.J. (2018), *Fatigue Fract. Eng. Mater. Struct.*, vol. 41, p. 894.
[16] Zhang, Z. and Wu, X.J. (2021), ASME. *J. Eng. Gas Turbines Power*, vol. 143, p. 1.
[17] Li, S.Q., Wu, X.J., Liu, R. and Zhang, Z. (2022), *SAE Int. J. Mater. Manuf*., vol 15, p. 1.
[18] Brommesson, R., Ekh, M. and Joseph, C. (2016), *Eng. Fract. Mech*., vol. 154, p. 57.
[19] He, J., Sandström, R. and Notargiacomo, S. (2017), *J. Mater. Eng. Perform*., vol. 26, p. 2257.
[20] Hill, R. (1948), *Proc. Soc. London Ser. A Math. Phys. Sci*., vol. 193, p. 281.
[21] Shah, D.M. and Duhl, D.N. (1984). In: *Superalloys 1984*, pp. 105–114.
[22] Lee, Y.-L. and Barkey, M. E., and Kang, H.-T. (2012). In: *Metal Fatigue Analysis Handbook*, p 253-297.
[23] Tomkins, B. (1975), *ASME J. Eng. Mater. Technol. Trans*, vol. 97, n. 4, p. 289, doi: 10.1115/1.3443301.
[24] ASTM-E739 − 10 (2015) - Standard Practice for Statistical Analysis of Linear or Linearized Stress-Life (S-N) and Strain-Life (ε-N) Fatigue Data, ASTM International, West Conshohocken.